LRP 504/94 October 1994

Papers presented at the Fifteenth International Conference on Plasma Physics and Controlled Nuclear Fusion Research

Seville, Spain, 26 September - 1 October 1994

LIST OF CONTENTS

INTERNATIONAL ATOMIC ENERGY AGENCY

FIFTEENTH INTERNATIONAL CONFERENCE ON PLASMA PHYSICS AND CONTROLLED NUCLEAR FUSION RESEARCH

Seville, Spain, 26 September – 1 October 1994

IAEA-CN-60/A-5-I-2

VARIABLE CONFIGURATION PLASMAS IN TCV

J.B. LISTER, F. HOFMANN, M. ANTON, S. BARRY, R. BEHN, S. BERNEL, G.BESSON, F. BUHLMANN, A. BURRI, R. CHAVAN, M. CORBOZ, M.J. DUTCH, B.P. DUVAL, D. FASEL, A. FAVRE, S. FRANKE, A. HEYM, A. HIRT, CH. HOLLENSTEIN, P-F. ISOZ, B. JOYE, X. LLOBET, J.C. MAGNIN, F.B. MARCUS+, B. MARLETAZ, PH. MARMILLOD, Y. MARTIN, J-M. MAYOR, J-M. MORET, CH. NIESWAND, P.J. PARIS, A. PEREZ, Z.A. PIETRZYK, R.A. PITTS, A. POCHELON, R. RAGE, O. SAUTER, G. TONETTI, M.Q. TRAN, F. TROYON, W. VAN TOLEDO, D.J. WARD and H. WEISEN

Centre de Recherches en Physique des Plasmas
Association EURATOM-Confédération Suisse
Ecole Polytechnique Fédérale de Lausanne
CH 1015 LAUSANNE Switzerland

+present address : JET, Abingdon, UK

VARIABLE CONFIGURATION PLASMAS IN TCV

ABSTRACT

During its first year of operation, TCV has achieved a wide variety of plasma shapes, limited and diverted, attaining 810 kA plasma current and elongation over 2.0. Ohmic H-Modes have been regularly produced, with a maximum confinement time of 80 msec and maximum normalised β_N of 1.9. The conditions for the H-Mode transition differ from other experiments. The transitions from ELM-free to ELMy H-Modes and back have been selectively triggered for configurations close to a Double-Null.

1. INTRODUCTION

The Tokamak à Configuration Variable, TCV, will explore the detailed effects of cross-sectional shaping on plasma performance. To be freely capable of producing widely different configurations, TCV is equipped with a set of 16 independently powered poloidal shaping coils, eight in a vertical stack on each side of the vessel, which has an almost rectangular aperture with a height/width ratio of 3.0 (Fig. 1). The constructional parameters of TCV are : R=0.88m, a=0.24m, height=1.44m, B_ϕ=1.43T. The vessel is completely carbon tiled over the inside and bottom walls and partly covered elsewhere.

Although the prime aims of TCV will only be achieved with the 4.5 MW of additional ECRH due to start commissioning in 1995, considerable progress has been made in plasma discharge control and particular attention has been paid to the nature of the transitions relating to Ohmic H-modes [1].

2. OPERATION AND PERFORMANCE

A symbolic q_a=6 plasma discharge was obtained in November 1992. The first full operational period (June-November 1993) was dedicated to discharge control and shaping. The shapes produced already covered a wide range of current, elongation and triangularity. The second operational period (February 1994-September 1994) saw the creation of fully diverted discharges with upper and lower Single-Nulls and Double-Nulls. The plasma current now extends up to 810 kA, the elongation to 2.05 and the triangularity varies from -0.7 to 0.8.

The shape parameters for each discharge are determined using a full equilibrium reconstruction code [2]. Different methods have been tested for real time discharge control, using the hybrid analog-digital TCV Plasma Control System. Shaping was controlled for most of the data in this paper using finite element reconstruction of the plasma current [3] and we have also developed control using heuristic flux combinations programmed by a Neural Network acquired knowledge base [4]. Vertical position has been controlled using several techniques, stabilising plasmas with growth rates up to 800 sec^{-1}. The power supply bandwidth has so far prevented us from exceeding this value. Interestingly, there has been no evidence for any increase in disruption likelihood as the growth rate increases, until the limit is reached and a disruption inevitably ensues.

In spite of the continuously welded vessel (Resistance 55 μΩ), plasma breakdown in TCV is reliably obtained between 7 and 10 volts per turn, assisted only by a hot filament at a potential of -900V. Plasma current ramps are typically ±1.5 MA/s, slightly slower than the plasma R/L rate. Shaping is performed during the current ramps and during the flat-top, according to the scenario required. Regular operation is achieved down to a value of q_{95}=2.0 with only rare problems encountered crossing q_{95}=3.

Ohmic H-Mode discharges were marginally obtainable in diverted discharges prior to boronisation. Following boronisation, ELM-free and ELMy H-Modes have been regularly and reproducibly obtained in limited and diverted deuterium discharges. H-Modes have lasted up to 1.5 seconds, and persisted into the plasma current ramp-down. ELM-free phases have lasted for up to 0.4 seconds.

The maximum line-averaged density achieved is 1.7×10^{20} m^{-3} and 100% of the Greenwald limit was obtained at the end of an ELM-free density rise.

The plasma energy confinement time is estimated from the total kinetic energy content, the Poynting vector at the plasma surface and the internal poloidal field magnetic energy, all determined by the plasma equilibrium reconstruction. The maximum energy confinement time was 80 msec, during the density rise of an ELM-free H-Mode. The ratio between the energy confinement time and the ITER89-P scaling varies from 0.5 to 1.4 for L-Mode discharges, due to a density dependence in the experimental data, and from 1-2.4 for H-Mode discharges. The normalised beta, $\beta_N=(\beta_{tor}aB/I_p)$ varies from 0.3 at low density to 1.9 for high density H-Mode discharges. The independent roles of plasma current, q_{95}, elongation, and triangularity on the confinement have not yet been unveiled in the presently rather inter-correlated database.

3. OHMIC H-MODE TRANSITIONS

An important aspect of the Ohmic H-Mode is the set of conditions required to obtain the L-H transition, which is always into an ELM-free H-Mode in TCV, and those subsequently required to enter an ELMy phase. In the ELM-free phase, the unavoidable increase in plasma density leads to a disruption if no ELMy phase ensues and no H-L transition occurs either spontaneously or provoked by a change in the configuration. The spontaneous ELMy phases have been more frequent after a fresh boronisation or after a helium glow.

At fixed plasma current and with a slow density ramp there is clearly a density threshold for the L-H transition. Above a minimum plasma current for the transition to occur at all, this density threshold did not vary with the plasma current for a given configuration, namely Single-Null-Upper (ion grad-B drift towards the X-Point). Different configurations have different line-averaged density thresholds, e.g. Single-Null-Upper at 3×10^{19} m^{-3} and Limiter at 7×10^{19} m^{-3}. The density threshold did not vary when the field and the plasma current were both reduced by 30%.

The H-Mode was not obtained for simple Single-Null-Lower discharges, but otherwise the precise role of the boundary shape on the density threshold is not yet clear. Within 100 μsec of the L-H transition seen on the D-alpha signal, a reduction of the MHD mode activity is observed, as well as a reduction of broad-band turbulence near the X-points [5].

The role of the power in determining the transition was seen in higher Z_{eff} conditions after a vent and before re-boronisation. The L-H transition into an ELM-free H-Mode started a density rise which ended on an H-L transition, Fig 2. The density dropped to its set value, the loop voltage and P_{oh} then decreased as the plasma cleaned up leading to a further L-H transition. This cycle repeated 7 times in a single discharge and suggests that the quantity P_{oh}/Surface-area alone does not determine our H-Mode transitions, which clearly occurred with this quantity both increasing and decreasing. The conducted power at the plasma edge was probably increasing in all cases, the radiated power dropping faster than P_{oh} as the plasma cleaned up, suggesting the conducted power as a more general candidate for the transition condition.

The triggering of the normally unpredictable ELM-free to ELMy transition was demonstrated in 2 Double-Null configurations i.e. both upper and lower X-points inside the vessel, one of which is shown in Fig. 3. The magnetic axis height was modulated repetitively (±1.2 cm), with roughly fixed shaping field, causing the shape to oscillate while retaining both X-points inside the vessel. The ELM-free to ELMy transition was triggered 7 times in this discharge, up to 18 in others, synchronously with the configuration modifications. Double-Null configurations might therefore appear to be particularly attractive if the H-Mode ELMy phase can also be controlled in the presence of additional heating using alternation between 2 very close equilibria close to a Double-Null.

ACKNOWLEDGEMENTS

It is a pleasure to acknowledge the support of the full TCV construction team in the first runs of this new experiment. This work was partly supported by the Swiss National Science Foundation.

[1] HOFMANN, F., LISTER, J.B., ANTON, M., BARRY, S., BEHN, R. et al., Proc. 21st EPS Conf. on Contr. Fusion and Plasma Physics, Montpellier, 1994 (to be published)
[2] HOFMANN, F., TONETTI, G., Nuclear Fusion 28 (1988) 1871
[3] HOFMANN, F., JARDIN, S.C., Nuclear Fusion 30 (1990) 2013
[4] LISTER, J.B., MARTIN, Y., MORET, J-M., Proc. 21st EPS Conf. on Contr. Fusion and Plasma Physics, Montpellier, 1994 (to be published)
[5] POCHELON, A., ANTON, M., BUHLMANN, F., DUTCH, M.J., DUVAL, B.P. et al., Proc. 21st EPS Conf. on Contr. Fusion and Plasma Physics, Montpellier, 1994 (to be published)

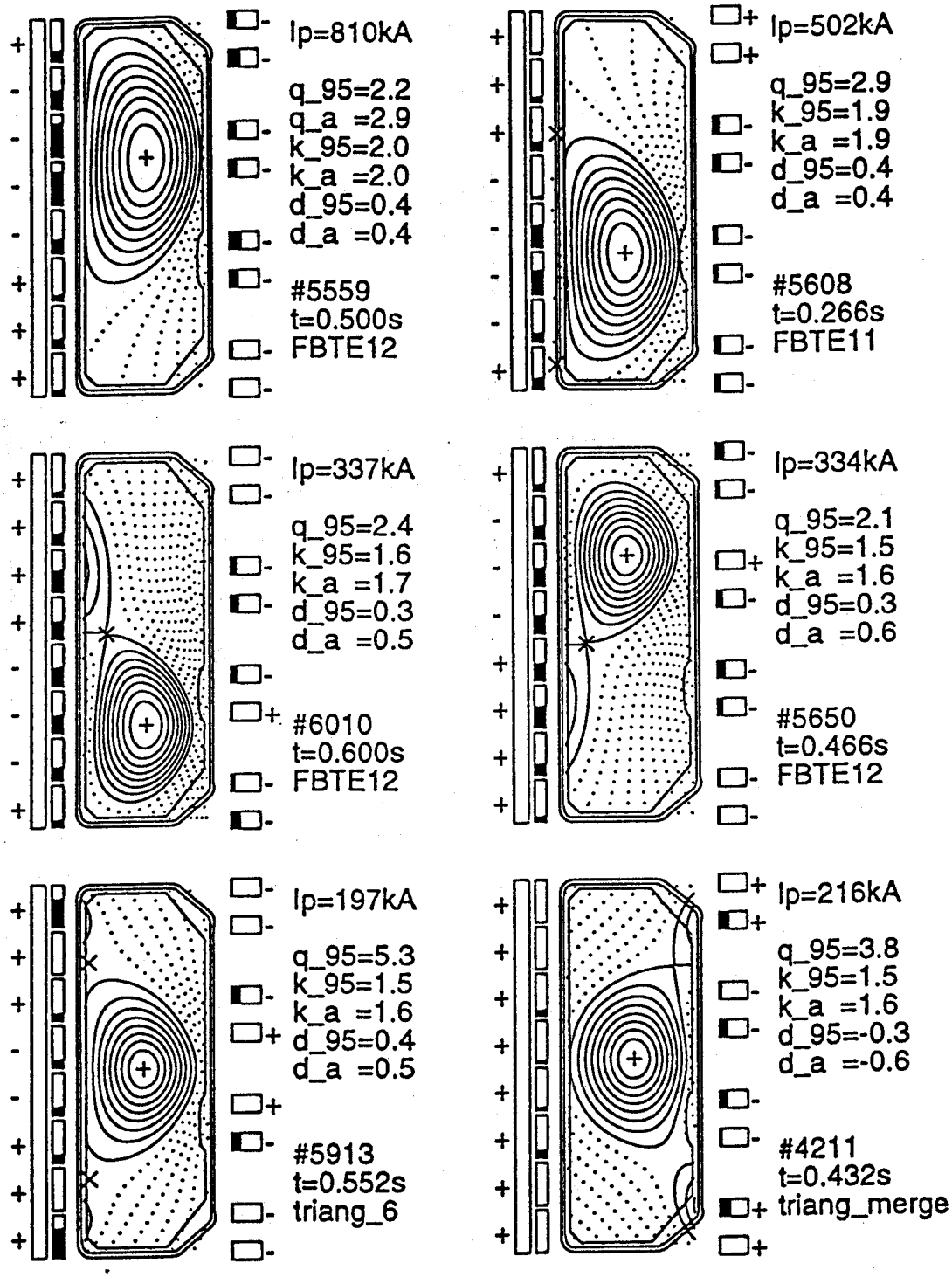

1. Various plasma shapes produced in TCV.

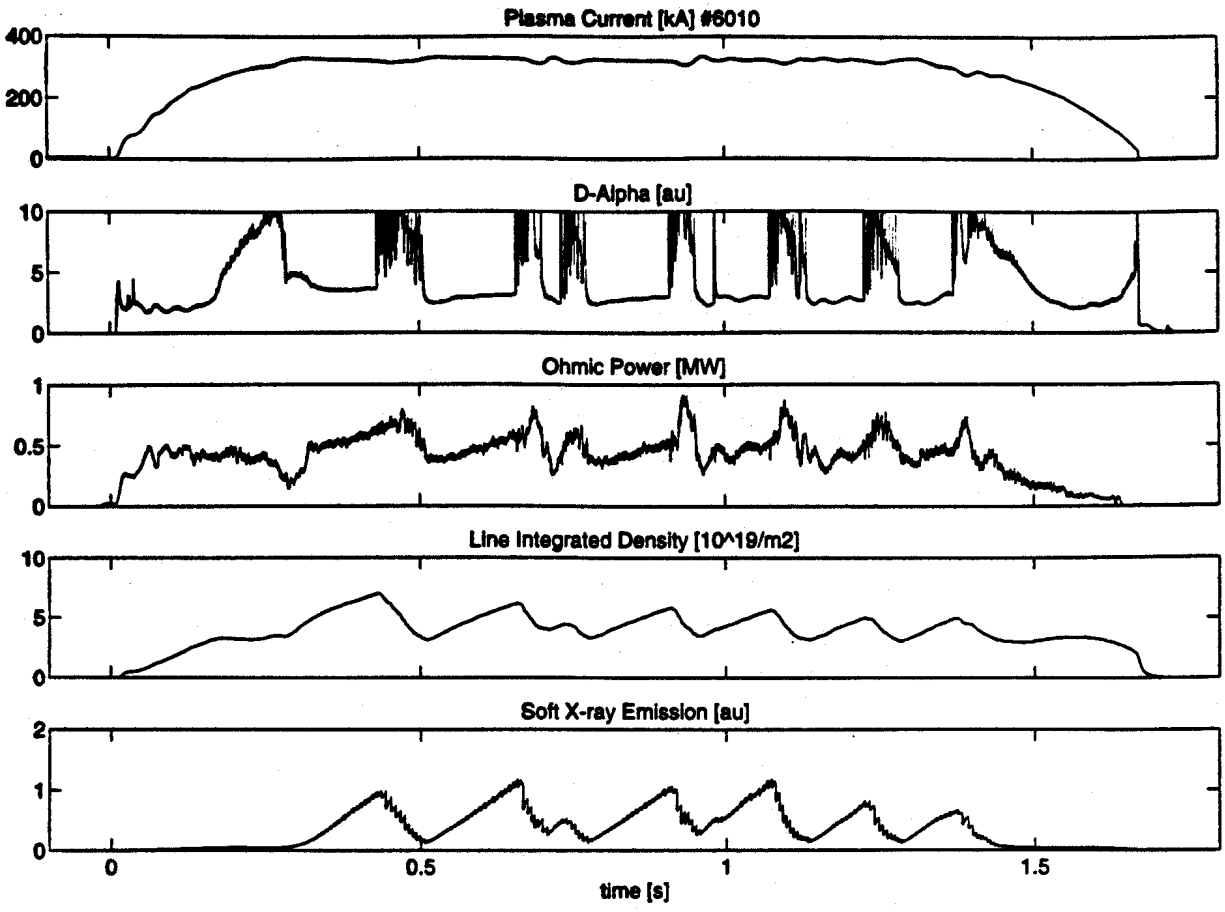

2. Repetitive L-H and H-L cycles with the L-H transitions occurring as the Ohmic Power decreases.

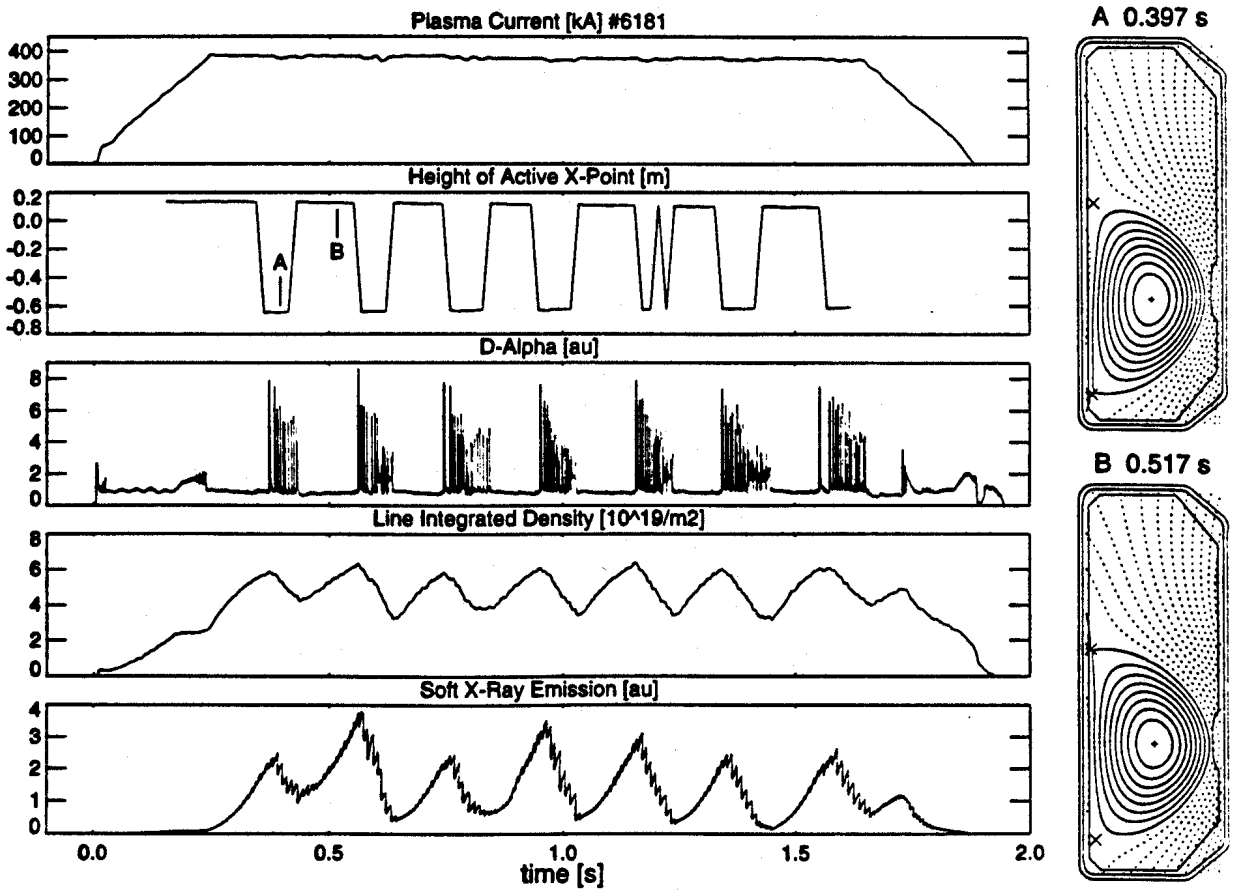

3. Modulation of the vertical position, causing small changes which trigger the ELM-free to ELMy transition and vice-versa.

INTERNATIONAL ATOMIC ENERGY AGENCY

FIFTEENTH INTERNATIONAL CONFERENCE ON PLASMA PHYSICS AND CONTROLLED NUCLEAR FUSION RESEARCH

Seville, Spain, 26 September – 1 October 1994

IAEA-CN-60/
D–I–3

Wall Stabilization of Ideal Modes in Tokamaks

D. J. Ward[1] and A. Bondeson[1,2]
[1]Centre de Recherches en Physique des Plasmas,
Association Euratom–Confédération Suisse, EPFL,
Lausanne, Switzerland
[2]Department of Technology, Euratom-NFR Association,
Uppsala University, Uppsala, Sweden

IAEA-CN-60/D-I-3

Wall Stabilization of Ideal Modes in Tokamaks

D. J. Ward[1] and A. Bondeson[1,2]
[1]Centre de Recherches en Physique des Plasmas,
Association Euratom–Confédération Suisse, EPFL, Lausanne, Switzerland
[2]Department of Technology, Euratom-NFR Association, Uppsala University,
Uppsala, Sweden

Abstract

We present two-dimensional stability calculations to show that low-n, pressure driven, external modes in tokamaks can be fully stabilized by resistive walls when the plasma rotates at some fraction of the sound speed. This stabilization can give significant increases in the beta limits imposed by these modes. The stabilization depends on the toroidal coupling of Alfvén and sound waves and is affected by ion Landau damping. This stabilizing effect is of particular importance to advanced tokamak configurations that depend on wall stabilization for low-n modes. Stabilization by resistive walls is found to be more effective in cases with more than one resonant surface in the plasma.

1. Introduction

In recent work [1], we have shown that it is possible to completely stabilize low-n, pressure-driven external modes in tokamaks by the combined effect of resistive walls and toroidal plasma rotation. For simple equilibria, we found that increases in the $n = 1$ beta limit of the order of 30% could be obtained when the plasma rotates at about 5% of the Alfvén speed. This offers a possible explanation of the beta values above the wall-at-infinity limit observed in the DIII-D tokamak [2]. To study the wall stabilization in toroidal geometry, we have modified the spectral codes MARS [3] and NOVA-W [4] to include a resistive shell in the vacuum region surrounding the plasma. Rigid toroidal rotation was modeled by making the resistive shell rotate with an imposed frequency $\omega_{\rm rot}$ while the equilibrium was static. The plasma was treated as ideally conducting, $\omega_{\rm rot}$ was some fraction of the sound frequency, and the time-constant of the resistive wall, τ_w, was taken much larger than any ideal-MHD timescale.

In the case of sonic rotation the stability problem includes inertia and the coupling of Alfvén and sound waves. Contrary to the MHD result, the sound waves are strongly damped by ion Landau damping in an isothermal plasma,

and an accurate description must be kinetic along the field lines. We have approximated such kinetic effects by adding dissipative terms to the fluid equations. One model is a damping of the Lagrangian pressure perturbations, i.e., we write:

$$p_1 = -\vec{\xi} \cdot \nabla p_0 + p_{1L}, \quad \text{with} \quad \partial p_{1L}/\partial t = -\Gamma p_0 \nabla \cdot \vec{v} - \nu p_{1L} \tag{1}$$

The damping rate ν is taken either to be a fixed number or to represent a thermal diffusivity following the Hammet-Perkins [5] prescription, $\nu = \chi |k_\parallel v_{\rm thi}|$. Alternatively, we use a parallel viscosity for the motion along the field lines:

$$\partial v_\parallel/\partial t = -(\vec{B} \cdot \nabla p)_1/B_0\rho_0 - \kappa |k_\parallel v_{\rm thi}| v_\parallel \tag{2}$$

2. Results

When the pressure exceeds the stability limit with the wall at infinity, we find two classes of modes that can potentially be unstable: (a) one which has zero frequency in the frame of the plasma and hardly penetrates the resistive wall: the "plasma mode"; and (b) one which penetrates the wall and rotates slowly with respect to it (slip frequency, $\Delta\omega_{\rm res} = O(\tau_w^{-1}) \ll \omega_{\rm rot}$): the "resistive wall mode." The resistive wall mode rotates with respect to the plasma at a frequency close to the imposed rotation frequency. A typical example of how the growth rates of the plasma and resistive wall modes depend on the wall radius d is shown in Fig. 1. The two modes are influenced in opposite ways by the wall distance—the plasma mode is *destabilized* as the wall is moved further from the plasma, while the resistive wall mode is *stabilized.*

The plasma mode rotates quickly (frequency $\approx \omega_{\rm rot} \gg \tau_w^{-1}$) with respect to the wall. It does not penetrate the wall and behaves as if the wall were ideal. The plasma mode is unstable on the ideal MHD time scale when the wall radius exceeds the usual ideal MHD threshold for wall stabilization, $d_{\rm ideal}$. This marginal wall position approaches infinity at the conventional beta limit and decreases with increasing pressure.

The resistive wall mode becomes increasingly stable with increasing wall radius. In Ref. [1] we presented a large-aspect-ratio model showing that such behavior should occur for a rotating plasma because the perturbation is forced to become complex at the continuum resonances ($d(\log \xi_m)/d\psi$ acquires an imaginary part). The model shows that the rotation separates the plasma and resistive wall modes, which behave in opposite ways with respect to the wall distance, and that the optimum wall position is some distance away from the plasma.

When a rotating plasma exceeds the pressure limit with the wall at infinity, there are two stability limits for the wall radius, $d_{\rm res}$ and $d_{\rm ideal}$ and the plasma is stable when $d_{\rm res} < d < d_{\rm ideal}$. The effect of wall stabilization is stronger when the pressure profile is broad so that the beta limit is set by external modes. An example is given in Fig. 2 which shows $d_{\rm ideal}$ and $d_{\rm res}$ for $n = 1$ versus normalized beta $g = \beta/(I_p[\mathrm{MA}]/a[\mathrm{m}]B_0[\mathrm{T}])$ at a rotation frequency $\omega_{\rm rot}/\omega_A = 0.06$. The computations were made for an equilibrium with JET shape (elongation = 1.7, triangularity = 0.3 and aspect ratio = 3) and a low pressure peaking factor, $p_0/\langle p\rangle \approx 1.7$. The current profile was adjusted to hold both $q_0 = 1.2$ and q_s fixed: $q_s = 2.55$ for the first sequence, and $q_s = 3.55$ for the second sequence. Stability limits are shown for the $n = 1$ resistive wall mode using the model of Eq. (1) with different damping coefficients. The stability boundaries are rather insensitive to the damping coefficient and the Hammett-Perkins approximation with $\chi = 2/\pi$ also gives a similar result. There is a region of stability in wall position between the boundaries for the two types of modes, which shrinks as the normalized beta is increased.

We find that when q_s is increased, holding the normalized beta and the pressure profile fixed, $d_{\rm res}$ for $n = 1$ moves closer to the plasma boundary. The stability limit in terms of normalized beta is higher at $q_s = 3.55$ than at $q_s = 2.55$ for both the resistive wall and the plasma mode. Increasing q_s to even higher values further increases the stable g.

There is presently considerable interest in advanced tokamak configurations [6], that have a bootstrap fraction near unity and are mainly in the second stability region to ballooning modes. Such equilibria are generally unstable to low-n, pressure-driven kink modes, unless they can be stabilized by a conducting wall. We have examined equilibria similar to those described in Ref. [6], with peaked pressure profiles, non-monotonic q-profiles with $q_0 = 2.5$ and $q_s = 3.7$, having only one integer q-surface ($q = 3$). We have compared these equilibria to similar ones with a somewhat larger region near the edge of positive shear, such that $q_s = 4.1$, which produces both a $q = 3$ and a $q = 4$ surface. Results are shown in Fig. 3 for the two sequences of equilibria. In both sequences, $q_0 = 2.5$ and $q_{\rm min} = 2.2$.

Results are given using both the simple pressure damping model, Eq. (1), and the parallel viscosity model, Eq. (2). For the equilibria with $q_s > 4$, both models predict a large region stable to both the plasma mode and the resistive wall mode with a suitable wall position and $\omega_{\rm rot}/\omega_A = 0.10$ up to $\beta^* \simeq 5\%$, where $\beta^* = 2\mu_0\langle p^2\rangle^{1/2}/\langle B^2\rangle$. An equilibrium that is stabilized in both models with the wall at $d/a \simeq 1.25$ has $q_s = 4.1$, $\beta^* = 4.7\%$, $g^* = 5.3$ (normalized β^*),

$\beta_p = 2.0$, a bootstrap fraction of 0.96, and the bootstrap current well aligned with the equilibrium current. By contrast, for the equilibria with $q_s < 4$, having only one resonant surface, stabilization by the resistive wall is not very effective. The resistive wall mode is much more stable for the equilibria with two resonant surfaces (when β^* is moderately above the wall-at-infinity limit). In fact, there is a larger region of stability for $q_s > 4$ with $\omega_{\rm rot}/\omega_A = 0.05$ than for $q_s < 4$ with $\omega_{\rm rot}/\omega_A = 0.10$. It is clear from Figs. 2 & 3 that the model of the sound-wave damping affects the quantitative results, but the dependence is not dramatic.

3. Conclusion

In summary, we have shown that low-n modes can be stabilized by resistive walls in combination with plasma rotation and that this leads to experimentally significant increases in the beta limit. The effect is more pronounced for broad pressure profiles and high q_s. A numerical example with standard q-profile and broad pressure profile shows an increase in the beta limit by about 30% – 40% due to the wall stabilization. MHD stability analyses indicate that similar increases are observed experimentally in DIII-D [2]. An increase by a factor of almost 2 in β^* can be achieved in advanced tokamak equilibria, and for such equilibria, sufficiently high values of q_s are needed for wall stabilization to be effective.

Acknowledgments

This work was supported in part by the Swiss National Science Foundation and by Euratom by the association contracts with Switzerland and Sweden.

References

[1] BONDESON, A., WARD, D.J., Phys. Rev. Lett. **72** (1994) 2709.

[2] TURNBULL, A.D., et al., Int. Sherwood Theory Conf., Dallas, TX, 1994, paper 2B1; and IAEA-CN-60/A-5-II-4, these Proceedings.

[3] BONDESON, A., VLAD, G., LÜTJENS, H., Phys. Fluids **B 4** (1992) 1889.

[4] CHENG, C.Z., CHANCE, M.S., J. Comput. Phys. **71** (1987) 124;
WARD, D.J., JARDIN, S.C., CHENG, C.Z., J. Comput. Phys. **104** (1993) 221.

[5] HAMMETT, G.W., PERKINS, F.W., Phys. Rev. Lett. **64** (1990) 3019.

[6] KESSEL, C., et al., Phys. Rev. Lett. **72**, (1994) 1212.

Figures

Fig. 1. Growth rate $\gamma_{\rm res}$ and slip frequency $\Delta\omega_{\rm res}$ vs. wall radius for $\omega_{\rm rot}/\omega_A = 0.06$.

Fig. 2. Marginal wall distance versus Troyon factor g for equilibria with the same pressure profile, with $q_s = 2.55$ and $q_s = 3.55$. (a)–(b) are the resistive wall mode boundaries for $q_s = 2.55$ with the pressure damping model, Eq. (1), with (a) $\nu/\omega_A = 0.025$ and (b) $\nu/\omega_A = 0.0025$. (c) and (d) are resistive wall mode boundaries for $q_s = 3.55$ equilibria with (c) $\nu/\omega_A = 0.025$ and (d) $\nu/\omega_A = 0.01$.

Fig. 3. Stability boundaries for equilibria with negative central shear and high bootstrap fraction. Results are shown for sequences with $q_s = 3.7$ (dashed curves) and $q_s = 4.1$ (unbroken curves). The ideal $n = 1$ boundaries are given by the solid squares, the $n = 1$ resistive wall mode boundaries using the parallel viscosity model, Eq. (2), and $\omega_{\rm rot}/\omega_A = 0.10$ are given by the open circles, while the simple pressure damping model (p. d. m.) results are the open triangles. The crosses represent the resistive wall mode boundary using the parallel viscosity model for the $q_s = 4.1$ sequence at half the rotation speed, $\omega_{\rm rot}/\omega_A = 0.05$.

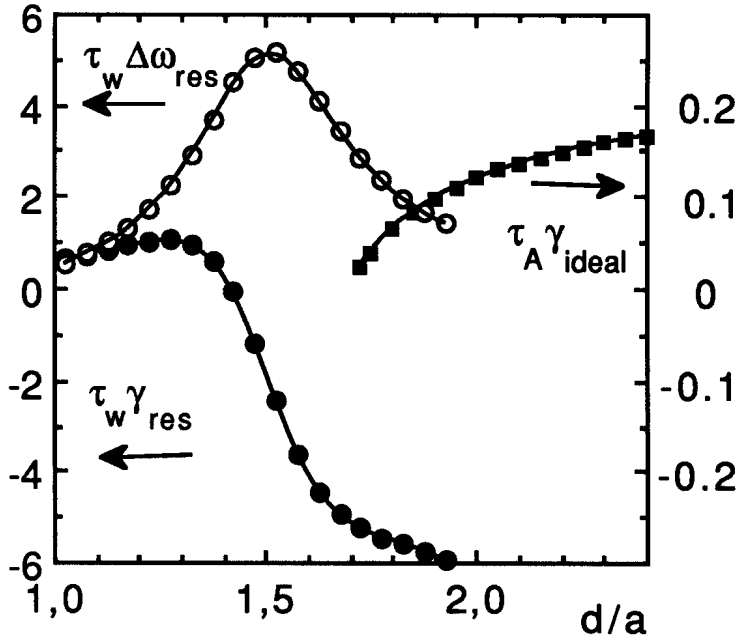

Figure 1.

Figure 2

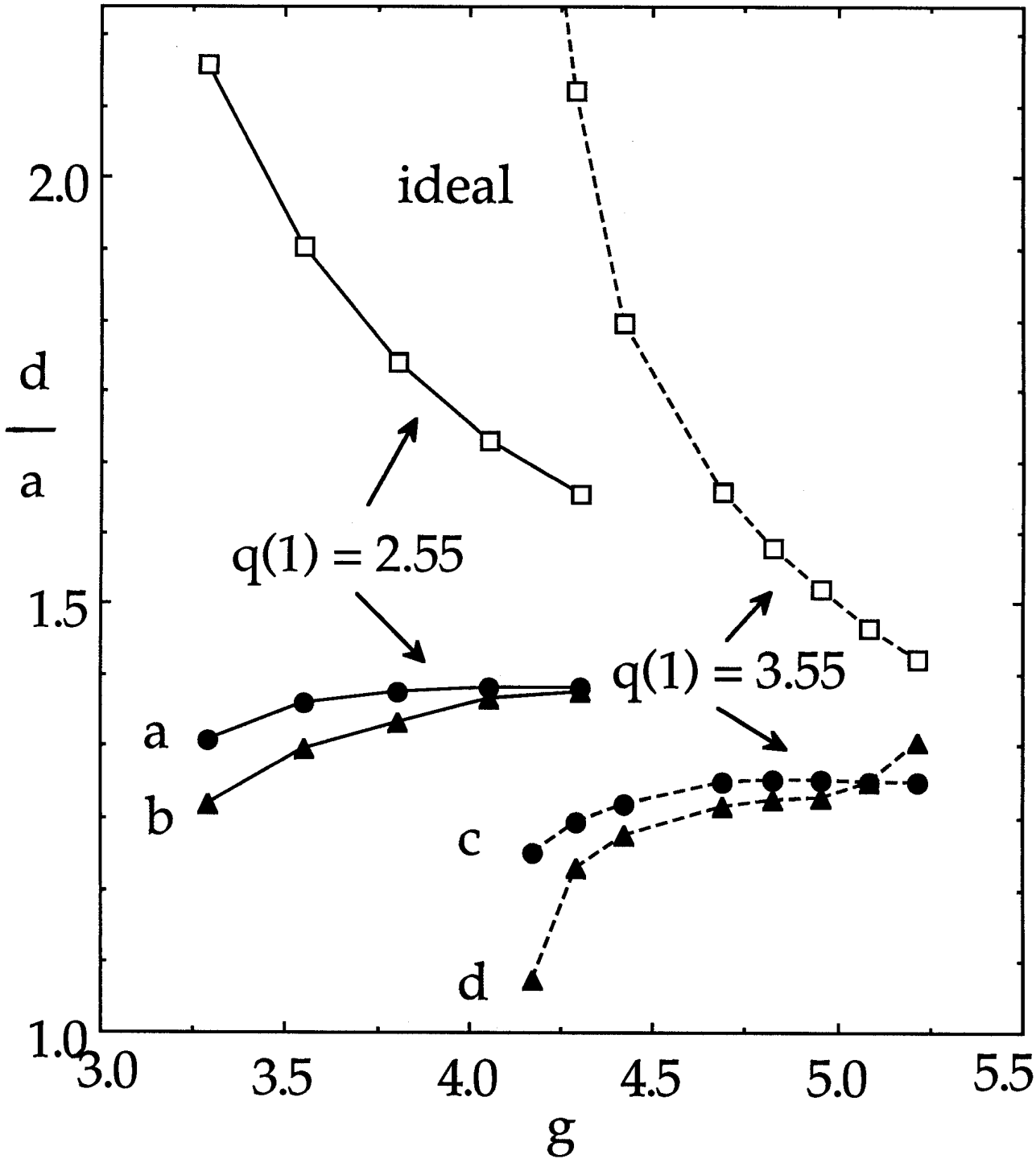

Figure 3

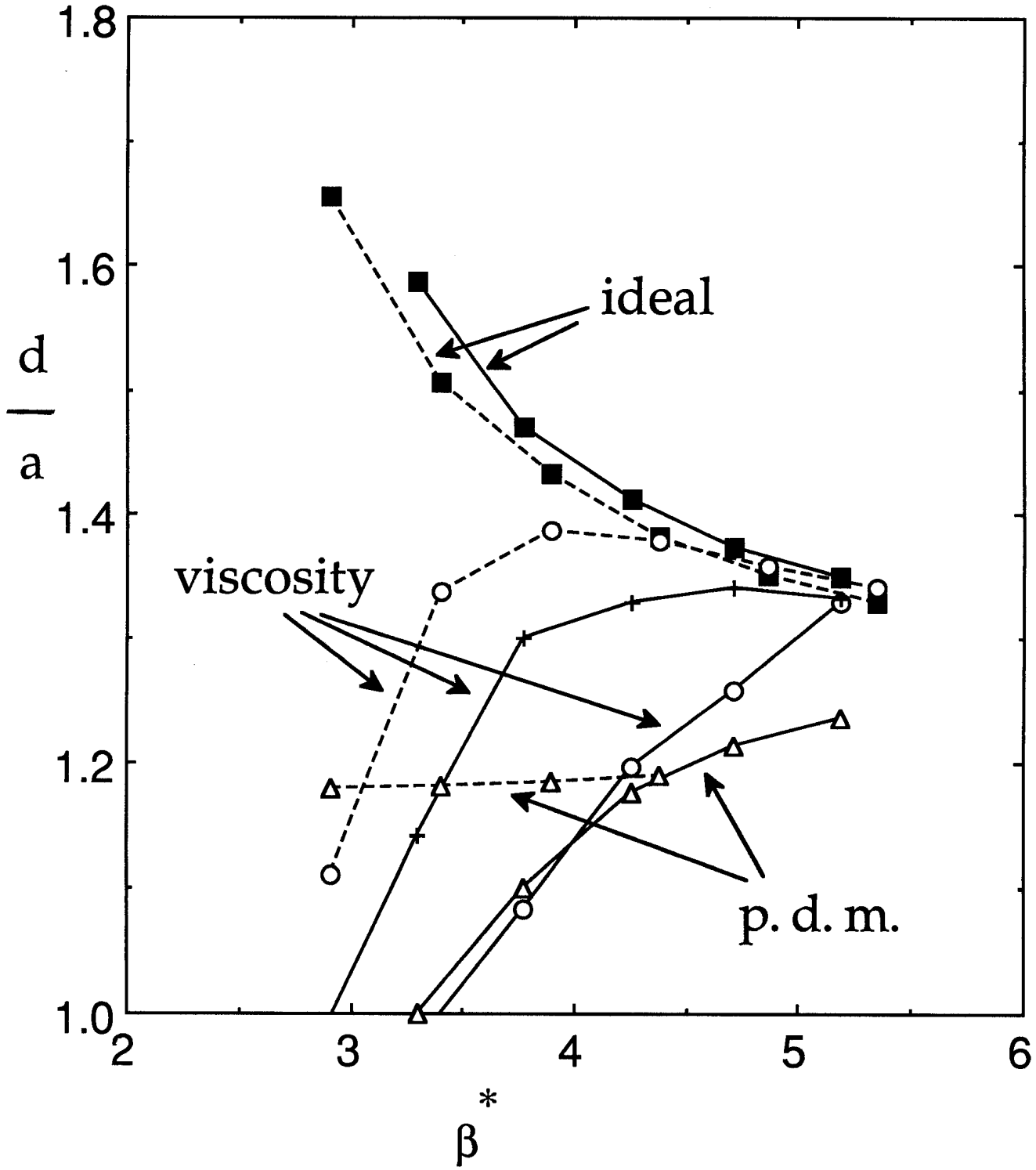

INTERNATIONAL ATOMIC ENERGY AGENCY

FIFTEENTH INTERNATIONAL CONFERENCE ON
PLASMA PHYSICS AND CONTROLLED NUCLEAR FUSION RESEARCH

Seville, Spain, 26 September - 1 October 1994

Post-Deadline Paper

Alfven Eigenmodes
Active Excitation Experiments in JET

by

A.Fasoli[1], S.Ali-Arshad, D.Borba, G.Bosia, D.Campbell, J.A.Dobbing, C.Gormezano, J.Jacquinot, P.Lavanchy[1], J.Lister[1], P.Marmillod[1], J.M.Moret[1], A.Santagiustina, S.Sharapov

JET Joint Undertaking, Abingdon, Oxon, OX14 3EA, UK
[1]CRPP/EPFL, 21 Av.des Bains, CH-1007 Lausanne, Switzerland

JOINT EUROPEAN TORUS JET

Post Deadline Paper

ALFVEN EIGENMODES ACTIVE EXCITATION EXPERIMENTS IN JET

A.Fasoli[1], S.Ali-Arshad, D.Borba, G.Bosia, D.Campbell, J.A.Dobbing, C.Gormezano, J.Jacquinot, P.Lavanchy[1], J.Lister[1], P.Marmillod[1], J.-M.Moret[1], A.Santagiustina, S.Sharapov

JET Joint Undertaking, Abingdon, Oxon, OX14 3EA, UK
[1] CRPP/EPFL, 21 av.des Bains, CH-1007 Lausanne, Switzerland

ABSTRACT

The newly installed JET Alfven Eigenmodes (AE) active diagnostic is described along with the first experimental results. The aim of this diagnostic, which is based on external antenna excitation and synchronous detection of the plasma response, is a systematic study of the AE properties, in particular in terms of damping and stability. Direct information on frequencies, mode structures and, most importantly, damping rates of the excited global resonances can be obtained. TAE modes have been excited and identified by the dependence of their frequency upon magnetic field and density. The first direct measurements of the AE damping rates in different regimes corresponding to distinct dominant absorption mechanisms are reported.

1. INTRODUCTION

The understanding of the interaction between magnetically confined toroidal plasmas and fusion generated alpha particles is one of the key issues in the preparation of thermonuclear ignition experiments. In tokamaks and stellarators, energetic particles generated by fusion reactions or additional heating can excite via resonant interaction global Alfven Eigenmodes (AE), which can in turn trigger anomalous fast particle losses [1]. The parameter space over which ignition and safe operation can be achieved may be limited in the presence of these instabilities both by the induced degradation of alpha confinement and by the possible first wall damage due to localised energy deposition by the mode scattered resonant particles [2]. The natural occurrence of Alfven Eigenmodes is related to the balance between different damping mechanisms and the fast particle driving. AE spectra, mode structures and instability thresholds can be investigated by simply observing fluctuations in the appropriate frequency range [1]. Energetic particles driven AE activity has been reported for NBI and ICRH heated discharges in different tokamaks, including JET [3]. These passive measurements, however, cannot provide quatitative information concerning damping and driving effects. A more comprehensive understanding of the MHD activity in the Alfven regime can be reached via a study of the plasma response to externally driven perturbations. External antenna excitation and coherent detection of different probing signals at the edge and in the plasma core are combined in the Alfven Eigenmodes active diagnostic at JET. Such a diagnostic has the unique advantage of providing a direct measurement of the damping rates of the Alfven Eigenmodes in different plasma conditions.

2. EXPERIMENTAL SET-UP

i) Active antenna excitation

The JET saddle coil antennas are used to excite the Alfven Eigenmodes. The launching apparatus, developed to cover the frequency range of pressure, toroidicity and ellipticity induced AE (30 to 500 kHz), encompasses a remotely controllable function generator, a 3 kW broad band power amplifier, an impedance matching network, a power distribution and an isolation unit. The power distribution unit connects the amplifier output to the active antennas,

allowing different combinations of antenna phasing that can preferentially excite specific toroidal and/or poloidal mode numbers (n: all, odd, even, (2,6,...), (4, 8,...); m: odd, even). Input current and voltage are measured at the distribution unit, whilst the voltage measurements on both the active and passive saddle coils are taken at the isolation unit. Currents on the saddle coils are measured at the end of the 80 m transmission line. Maximum currents and voltages induced in the saddle coils by the AE exciter in the present configuration are of the order of 30 A and 500 V, respectively. Correspondingly, the magnetic perturbations in the plasma are predicted to be such that $\delta B/B<10^{-5}$. As a result, the excited AE amplitudes are not expected to enhance the transport of energetic particles.

ii) Diagnostic method

The excitation frequency is swept across the shear Alfven gap regions, where AE are expected. The plasma response is extracted from background signals via homodyne detectors, providing in phase and quadrature components of the signals, or, in a complex representation, their real and imaginary parts. Different probing channels are considered: The voltage and current of the excited saddle coils provide the antenna impedance. The induced voltage on the passive saddle coils and the fast magnetic coils measure the perturbation of the radial and poloidal B-fields, allowing a mode analysis both in the poloidal and toroidal conjugate planes. Other non-magnetic diagnostics, such as heterodyne ECE and reflectometry, will be coupled to the synchronous detectors to reconstruct the radial structure of the excited global mode.

3. DATA ANALYSIS AND REPRESENTATION

The antenna-plasma-detectors transfer function can be directly obtained by dividing the complex amplitude of the different probes response by that of the current driven in the active antenna. The individual AE manifest themselves as resonances in the transfer function, which can be expressed as

$$H(\omega)=\frac{a+ib\dfrac{\omega}{\omega_0}}{1-\left(\dfrac{\omega}{\omega_0}\right)^2+i\dfrac{2\gamma}{\omega_0}\dfrac{\omega}{\omega_0}}$$

where ω is the angular frequency of the exciter signal, ω_0 the resonance (real) frequency and γ the damping rate. a and b are real numbers that, for small damping ($\omega_0>>\gamma$), are proportional to the in phase and quadrature components of the detected signals. To represent the plasma resonance in terms of complex conjugated poles (p, p*) and residues (r, r*), the complex transfer function H is decomposed in partial fractions. If several (N/2) resonances occur in the measurement range, this representation reads

$$H(\omega,x)=\sum_{n=1}^{N/2}\frac{1}{2}\left(\frac{r_n(x)}{i\omega-p_n}+\frac{r_n^*(x)}{i\omega-p_n^*}\right)=\frac{B(x)}{A}$$

where $p=i\omega_0+\gamma$ and x indicates explicitly the space dependence of a diagnostic signal. B and A denote polynomials in $i\omega$ with real coefficients and degree N-1 and N, respectively. For a given resonance only the numerators (the residues) depend upon the position, whilst the denominators, i.e. the poles, are common. Since the signals may contain direct coupling with the antenna, an additional quantity, dependent upon position, must be added

$$H(\omega,x)=\frac{B(x)}{A}+D(x)=\frac{B'(x)}{A}$$

B'(x) can have a higher degree than B(x) to account for the antenna-probe coupling transfer function. The data analysis, based on the fit of a set of space resolved measurements of complex transfer functions with rational functions in $i\omega$ with real coefficients [4], leads to a representation of the eigenmodes in terms of complex poles and of the corresponding space dependent residues. The latter correspond to a measurement of the wave amplitude as a function of space, i.e. of the single mode structure. The pole provides two pieces of information. Its imaginary component gives the actual frequency of the mode, ω_0. When no fast particle driving terms are present in the plasma, the real part of the pole, γ, corresponds directly to the damping rate. For modes which are stable but for which a finite fast particle induced growth rate exists ($\gamma_{drive} \neq 0$, $\gamma_{damping} > \gamma_{drive}$), γ is the difference between the damping rate and the growth rate: $\gamma = \gamma_{damping} - \gamma_{drive}$. The cases of marginally stable ($\gamma_{drive} \sim \gamma_{damping}$) and unstable modes ($\gamma_{damping} < \gamma_{drive}$) are more complicate and would necessitate a data analysis in terms of non-linear models. Note that the synchronous detection chain can also be used in passive mode, with the reference frequency being swept across the expected AE frequency domain, but with no current driven in the saddle coils. In this case the frequency and amplitude of an unstable mode can be estimated, but, due to the lack of knowledge of the driving source spectrum, no information on its damping can be gathered.

4. FIRST EXPERIMENTAL RESULTS

i) Passive studies

Preliminary passive studies using two saddle coils and five magnetic probes indicated some broad band ($\Delta f > 30$ kHz) activity around the TAE frequency, f_{TAE}, when neutral beam heating at moderate power is applied to the JET diverted plasmas ($f_{TAE} \equiv v_{Alfven}/(4\pi q R_0)$ and $v_{Alfven} = B/(4\pi n_i m_i)^{1/2}$) . These studies helped in identifying the frequency domain of interest for the first phase of the active studies, which have subsequently been undertaken in the range 60-180 kHz.

ii) Results with active AE excitation

In this region several Eigenmodes have been clearly observed in the ohmic phases of JET pulses in different plasma configurations. An example of a resonance seen in an ohmic plasma is shown in Fig.1. When the frequency is swept across the resonance, the magnetic probe signal amplitude describes a circle in the complex plane. The maximum value of the perturbed magnetic field measured by the pick-up coil is of the order of 10^{-6} T. The relatively low damping rate ($\gamma/\omega \cong 1\%$) seems to suggest the absence of continuum damping.

iii) Eigenmode identification

To verify the 'Alfvenic' character of the observed resonance, the dependence of the observed resonance frequency upon the magnetic field and density was investigated. In the first case (Fig.2) only the toroidal magnetic field is varied. The measured frequency agrees with f_{TAE} calculated with the simplifying assumption that $q=1.5$, which for realistic JET profiles corresponds to the most unstable TAE mode [5]. The damping coefficient is not observed to vary throughout the scan. Fig.3 shows a case in which the density is varied, with toroidal field and plasma current practically constant. The observed mode frequency follows the calculated f_{TAE}. These two results clearly show that the observed resonances are related to the Toroidal Alfven Eigenmodes. Quality factors ($Q = \omega/\gamma$) of the order of ten at the beginning of the scan suggest that in this regime continuum damping can be responsible for the mode absorption. After $t \cong 49$s, the profiles are modified in such a way that $n(r)q^2(r)$ becomes approximately constant, and a second regime, in which the Alfven gaps are open and no continuum damping is possible, is entered.

iv) Effect of variations in the plasma current

A scan in the plasma current, for constant toroidal field, was performed in shot #31638. Variations in the mode frequency as well as in its damping coefficient clearly appear in the AE data (Fig.4). The observed frequency does not follow the simply calculated f_{TAE}, for fixed values of q and for densities taken at the corresponding radial position, but it increases as the plasma current is raised. The mode structure does not vary significantly throughout the scan, as shown in the poloidal reconstruction reported in Fig.5 for two different times. An increase in the plasma current produces an outward displacement of the resonant surface corresponding to a fixed value of q (e.g. q=1.5). The corresponding variation of the density along the radial profile would translate into a variation of v_{Alfven}, and thus of f_{TAE}, which is compatible with the observed Eigenmode frequency variation. A quality factor larger than 100 seems to exclude the presence of continuum damping for this shot and is consistent, for its order of magnitude and its variation with the density, with the predicted effect of electron Landau damping [6].

v) Effect of additional heating

Preliminary results concerning AE excitation in the presence of fast particles generated by NBI and/or ICRH indicate that the damping rate is changed by additional heating. Experiments with the AE active diagnostic in conjunction with NBI, IRCH and Lower Hybrid additional heating, current drive and profile control, are under way.

5. CONCLUSIONS

The combination of external antenna excitation and synchronous detection of the plasma response constitutes the basis of the Alfven Eigenmode active diagnostic at JET. The experimental apparatus has been installed and tested and the diagnostic method has been successfully demonstrated. MHD global modes have been excited and identified as Alfven Eigenmodes by the dependence of their frequency upon the density and the toroidal magnetic field. The damping rates of TAE modes have been experimentally measured for the first time. Control of antenna phasing and space resolved magnetic measurements allow a determination of the excited mode structure. These experimental investigations on the behaviour and specifically on the damping, of the Alfven Eigenmodes in JET, complemented by MHD and kinetic modelling, are expected to provide an important contribution to the assessment of the Alfven Eigenmode stability in future thermonuclear experiments.

REFERENCES:

[1] A.D.Turnbull et al., *Phys. Fluids B* 5, 2546 (1993).
[2] H.L.Berk et al., IAEA/D-P-II-1, *these proceedings.*
[3] S.Ali-Arshad and D.Campbell, to be published on *Plasma Phys. and Controlled Fusion.*
[4] J.-M.Moret, *CRPP Laboratory Report* LRP 498/94 (1994).
[5] L.Villard et al., *Proc. 20th Eur. Conf. on Controlled Fusion and Plasma Physics,* ed. by J.A.Costa Cabral, M.E.Manso, F.M.Serra, F.C.Schuller, EPS Lisbon, (1993) IV, 1347, and G.T.Huysmans et al., *ibidem,* I, 187.
[6] R.Betti and J.P.Freidberg, *Phys. Fluids B* 4, 1465 (1992).

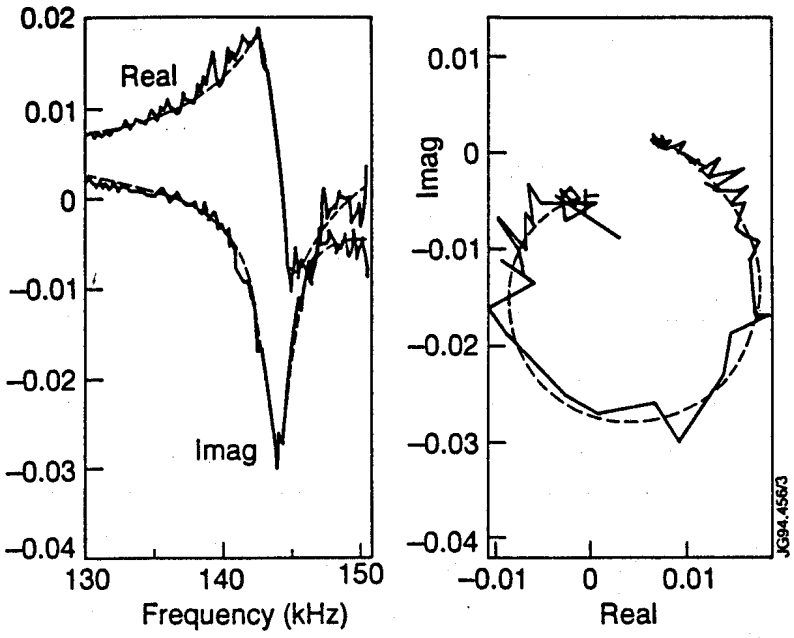

Fig.1 *Example of experimentally observed TAE resonance in the ohmic phase of JET shot #31638. Left: Real and imaginary part of a magnetic probe response. Right: Complex plane representation of the same signal. In both cases the signal is normalised to the exciter current. A fit with a rational fraction of order 5/2 is also shown. The fit gives f=144.2 kHz (δf<100 Hz), γ=1400 s^{-1}($\delta\gamma$<100 s^{-1}). B ≅ 2.8 T, I_p ≅ 2.2 MA, line integrated density ≅ $7x10^{19}$ m^{-3}. Two active saddle coils (on the top of the machine, in opposite octants, 1 and 5) with the same phase are used.*

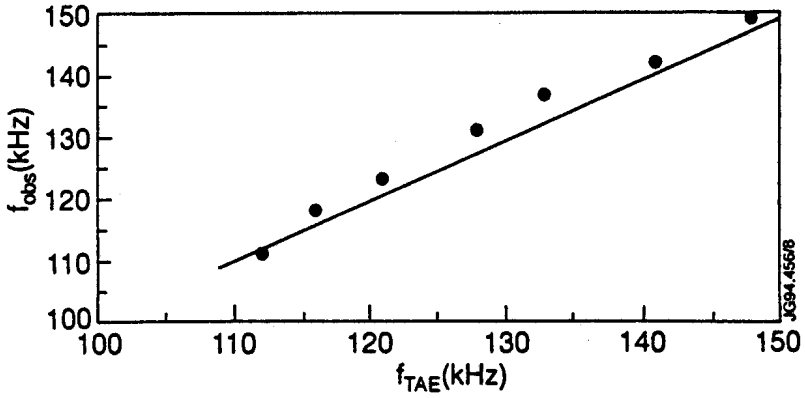

Fig.2 *Variation of the measured Eigenmode frequency with toroidal magnetic field (#31591). In the interval considered B is varied linearly between 2.2 T and 3 T. The density and plasma current are kept constant. The same saddle coils as in Fig.1 are active, but with opposite phase. Here and in Fig.3, f_{TAE} is calculated for constant q (q=1.5).*

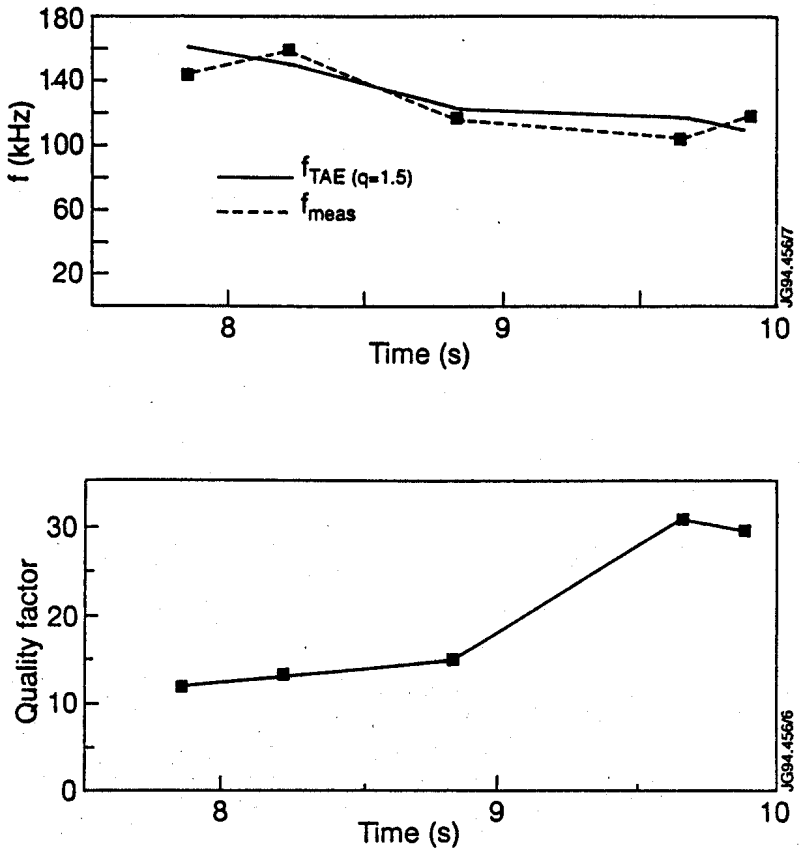

Fig.3 *TAE frequency (top) and quality factor (bottom) for different densities within JET shot #31150. The line integrated density varies between $5.2x10^{19}$ m^{-2} and $11x10^{19}$ m^{-2}; $B \cong 2.7$ T, $I_p \cong 2$ MA. One active saddle coil on the top is used.*

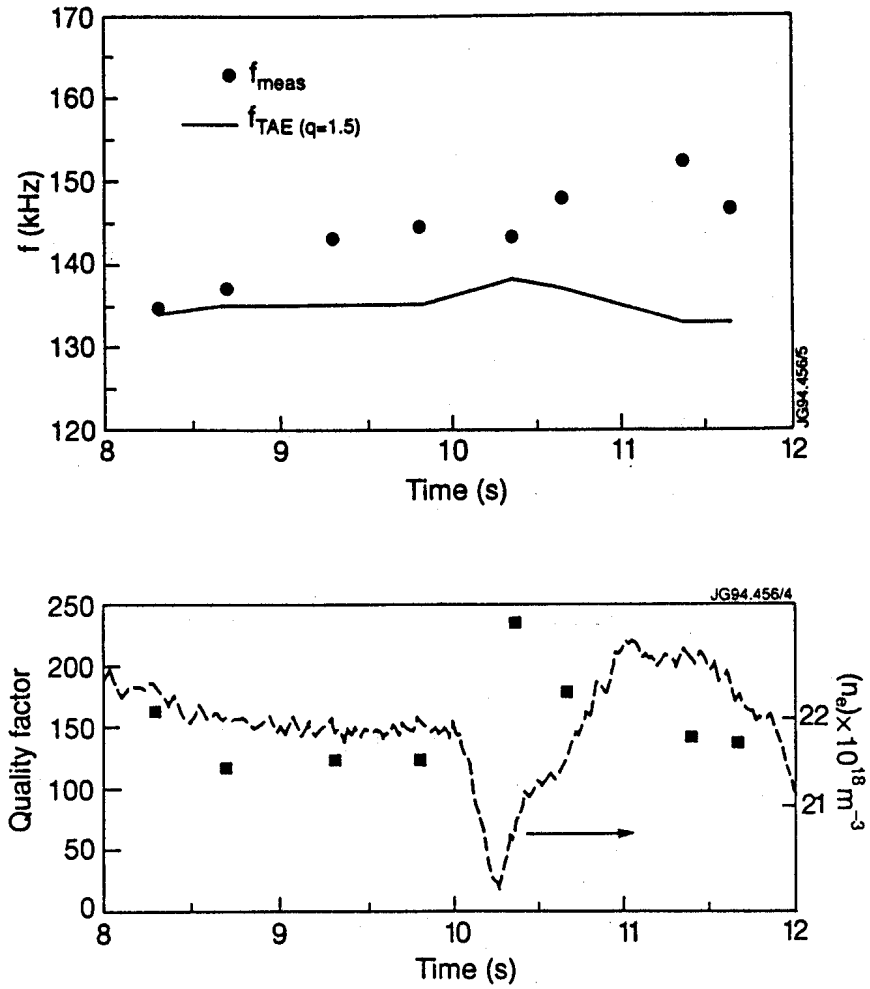

Fig.4 *Evolution of the observed frequency (top) and quality factor (bottom) of a global Alfven mode with increasing plasma current (JET shot #31638, as for Fig.1). The variation of density is also indicated (bottom). I_p is scanned linearly from 2.17 MA to 2.6 MA; $B \cong 2.8$ T.*

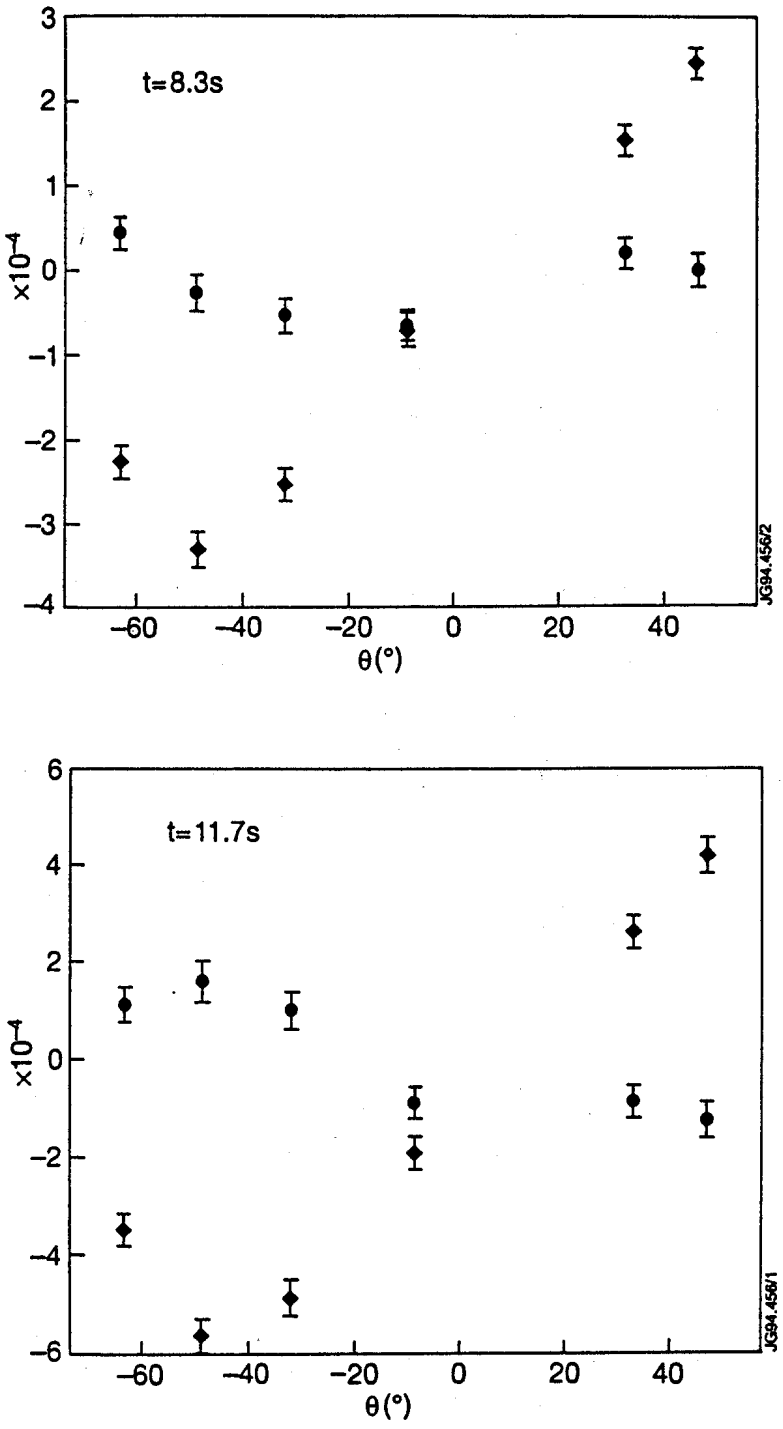

Fig.5 *Poloidal mode structure reconstruction for two different times of the current scan reported in Fig.4. Top: t=8.3 s; Bottom: t=11.7 s. Real (•) and imaginary (◆) components of the Eigenmode residues are plotted vs. the poloidal angle. As in Fig.1 the magnetic signals are normalised to the active saddle coil current.*